Published in final edited form as:
ACS Nano. 2010 February 23; 4(2): 699–708. doi:10.1021/nn901146y.

In vivo Biodistribution and Clearance Studies using Multimodal ORMOSIL Nanoparticles

Rajiv Kumar[†], **Indrajit Roy**[†], **Tymish Y. Ohulchanskky**[†], **Lisa A. Vathy**[†], **Earl J. Bergey**[†], **Munawwar Sajjad**[‡], and **Paras N Prasad**[†,*]

[†]Institute for Lasers, Photonics and Biophotonics, The State University of New York at Buffalo, Buffalo, NY 14260

[‡]Department of Nuclear Medicine, The State University of New York at Buffalo, Buffalo, NY 14260

Abstract

Successful translation of the use of nanoparticles from laboratories to clinics requires exhaustive and elaborate studies involving the biodistribution, clearance and biocompatibility of nanoparticles for *in vivo* biomedical applications. We report here the use of multimodal organically modified silica (ORMOSIL) nanoparticles for *in vivo* bioimaging, biodistribution, clearance and toxicity studies. We have synthesized ORMOSIL nanoparticles with diameters of 20-25 nm, conjugated with near infra-red (NIR) fluorophores and radiolabelled them with ^{124}I, for optical and PET imaging *in vivo*. The biodistribution of the non targeted nanoparticles was studied in non-tumored nude mice by optical fluorescence imaging, as well by measuring the radioactivity from harvested organs. Biodistribution studies showed a greater accumulation of nanoparticles in liver, spleen and stomach than in kidney, heart and lungs. The clearance studies carried out over a period of 15 days indicated hepatobiliary excretion of the nanoparticles. Selected tissues were analyzed for any potential toxicity by histological analysis, which confirmed the absence of any adverse effect or any other abnormalities in the tissues. The results demonstrate that these multimodal nanoparticles have potentially ideal attributes for use as biocompatible probes for *in vivo* imaging.

Keywords

ORMOSIL Nanoparticles; optical and PET Imaging; NIR fluorophore; ^{124}I radiolabeling; Biodistribution; clearance and toxicity

Nanomaterials promise to address the current limitations of sensitivity and specificity of medical diagnostics, as well as significantly improve the outcome of existing and emerging therapeutics, via the introduction of new generation of multimodal nanoprobes.[1-6] In this regard, it is critical to design nanoprobes with desired composition, size and surface functionalities, and rigorously test them *in vitro* and *in vivo* for their safety and efficiency. Also biocompatibility and biodegradation of the nanoprobe materials play an important role in the use of the nanoprobes in the field of diagnostic and therapeutic applications.

The rise in nanoprobes development has bolstered the prospects of *in vivo* optical imaging through the development of a variety of NIR-luminescent nanoformulations, which include quantum dots,[7] upconverting nanophosphors,[8] and luminophore-containing nanoparticulate

*Corresponding Author: pnprasad@buffalo.edu.

Supporting Information **Available:** Description of the experimental details, and MTS assay results. This material is available free of charge via the Internet at http://pubs.acs.org.

carriers such as liposomes,[9] polymersomes,[10] ceramic,[11, 12] or polymeric[13, 14] nanoparticles, etc. Silica and organically modified silica (ORMOSIL) nanoparticles have several attributes that facilitate their use as a platform for the fabrication of an ideal nanoprobe. Ultrafine (diameter below 20 nm) nanoparticles of silica/ORMOSIL can be easily synthesized in a user-friendly and cost-effective manner, using microemulsion medium and ambient conditions. These materials are inert, non-antigenic, and have excellent storage stability and resistance to biofouling. They are optically transparent, and can serve as excellent optical probes, following the encapsulation/conjugation of fluorophores such as organic dyes or quantum dots.[15, 16] Such nanoincorporation protects the fluorophores from photobleaching, and prevents their interaction with the biological environment, thus potentially allowing a safe use of even toxic fluorophores.[17] In addition, the rich surface chemistry of silica/ORMOSIL allows the co-incorporation of other diagnostic probes for multimodal bioimaging, as well as suitable biorecognition molecules for target-specific delivery.[18]

Using silica/ORMOSIL nanoparticles encapsulated/conjugated with fluorophores and targeting ligands, our group and others have already demonstrated efficient optical imaging of tumor cells *in vitro*.[15, 19] In addition, we have synthesized ORMOSIL nanoparticles co-encapsulating quantum dots and iron oxide nanoparticles, and have shown their *in vitro* target specificity by using a synergistic combination of receptor-mediated targeting and magnetic guidance.[20] Finally, we have also developed ORMOSIL nanoparticles for a variety of therapeutic applications, which includes photodynamic therapy (PDT) of cancer and non-viral gene delivery.[21, 22] No adverse effects were observed when these nanoparticles have been directly introduced in the brain of live mice and rats. These promising observations have prompted us to investigate in detail the biodistribution and eventual fate of multimodal ORMOSIL nanoparticles *in vivo*, following systemic delivery. Such an investigation is critically important for the eventual application of these nanoprobes for routine clinical use in diagnostics and therapeutics.

Herein, we report the synthesis of ultrafine ORMOSIL nanoparticles (diameter ~20 nm), conjugated with a near-infra-red (NIR) fluorophore, as optical probes. The resulting NIR-nanoparticles will facilitate optical bioimaging in the NIR window, with maximum tissue penetration of light and minimum background signal.[23, 24] Furthermore, we have also conjugated the well-known positron emission tomographic (PET) imaging probe Iodine-124 with the nanoparticle, which will allow bioimaging independent of tissue-depth, as well as more accurate quantification of accumulation of nanoparticles in various major organs *in vivo*. These multimodal nanoprobes have been injected systemically in mice, and their *in vivo* biodistribution studies have been carried out, based on the acquisition of fluorescence emission of the conjugated fluorophore and the gamma emission of the conjugated ^{124}I. The clearance of the nanoparticles from the animal body, as well as long-term toxicity involving the affect of the nanoparticles on the major organs, has also been studied. The results indicate that these nanoparticles slowly clear out of the animal body via the hepatobiliary excretion, without causing any overt toxicity and tissue damage. Thus, it can be concluded that these multimodal nanoparticles have potentially ideal attributes for use as safe and efficient probes for *in vivo* bioimaging.

Results and Discussion

The nanoparticles characterization results are shown in figure 1. Figure 1a and 1b shows the size and distribution of the nanoparticles by DLS and TEM, respectively. DLS has shown the nanoparticles to be of unimodal distribution with the maximum percentage intensity to be of 20nm in size. TEM shows a good correlation with DLS showing the nanoparticle diameter to be around 20nm. As can be visualized from the TEM image, the nanoparticles have a spherical morphology with a narrow size distribution. The overall surface charge of the nanoparticles

was found to be negative with an absolute zeta potential value of −25.5mV. The negative surface charge can be attributed to the presence of the PEG molecules and a small amount of remnant anionic surfactant, AOT, on the surface of the nanoparticles. The net surface charge of the nanoparticles have a pronounced effect on the adsorption of different physiological lipoproteins in systemic circulation and plays a critical role in the clearance of the nanoparticles form the animal body.[3] It was also observed that upon incubation with the serum media, the nanoparticle size increased by more than 15nm in diameter, suggesting the binding of the serum proteins to the nanoparticles (data not shown).

Figure 1c shows the photophysical characterization of the OMROSIL nanoparticles with conjugated NIR dye DY776. The optical absorbance and fluorescence spectra of the nanoparticles showed an absorbance peak with λ_{max} at 780 nm and emission peak at 815 nm. No considerable shift in the emission wavelength was observed for the DY776-NHS ester, DY776-silane and DY776 conjugated nanoparticles, suggesting that the dye remained stable even after conjugation with the nanoparticle. Since both the excitation and emission wavelengths of the DY776 lie in the NIR region, the nanoparticle formulation offers an added advantage of autofluorescence-free *in vivo* imaging, as well as deeper penetration of the excitation and emission light. Figure 1d shows the normalized fluorescence decay curve of the aqueous suspension of the DY776 conjugated nanoparticles. From the fluorescence life time decay studies the average decay time was estimated to be 62.0ns, which indicates that decay time of the DY776 conjugated ORMOSIL nanoparticles is comparable with other optical based diagnostic probes frequently used for real time and long term imaging studies.

The biodistribution of ORMOSIL nanoparticles has been studied by two methods, one involving the fluorescence of the NIR fluorophore DY776 conjugated with the nanoparticles, and the other by radioactivity measured from the ^{124}I-labelled with the nanoparticles. For the *in vivo* fluorescence imaging a semi-quantitative approach was used, involving fluorescence quantification acquired from the dissected tissues as a percentage of the fluorescence from the injected dose (details in supporting information). Figure 2 shows the biodistribution profile of the ORMOSIL nanoparticles in nude mice. As can be seen from figure 2a, almost 75% of the injected dose accumulated in the liver and spleen, whereas the lung, kidney and heart accounted for minimum accumulation (less than 5%). High fluorescence recorded from the highly perfused organs, such as liver and spleen, could be accounted for as the combined activity of the circulating blood passing through organs, as well as that due to particle uptake by cells of the reticuloendothelial system (RES) recruited by these organs. It is interesting to note that a considerable amount of the nanoparticles go to the stomach and intestine (~8%), which can be attributed to the excretion of the nanoparticles over a period of 24 hrs. It is also observed from the figure that almost 9% of fluorescence was acquired from the skin, which can be corroborated to the possible fact that DY776 can direct the nanoparticles to the skin. This is further confirmed when the free DY776 was injected and a major percentage of fluorescence was observed from the skin (Supporting Information).

Figure 2b shows via PET imaging the biodistribution profile of the mice, intravenously injected with ^{124}I labeled nanoparticles over a period of 2-24hrs. The PET images showed a very similar pattern of uptake of the nanoparticles as was obtained from the fluorescence imaging of the mice. From the images, it can be easily visualized that major percentage of nanoparticles accumulated in the liver and spleen. A quantitative assessment of radioactivity of the injected ^{124}I labeled OMROSIL nanoparticles is shown in figure 2c. As shown in the figure, liver and spleen were the major host organs for the ^{124}I ORMOSIL nanoparticles. Quantitatively, a majority of the nanoparticles accumulated in spleen (from 58% of the injected dose per gram of the organ, at the first 5 min after intravenously injection to 61% at 24 h), followed by liver (from 37% to 46%), lungs (from 9.6% to 4.7%) and kidney (from 1.93% to 1.22%).

The comparison between the biodistribution profile obtained from the two methods showed a contrast in liver to spleen uptake which can be attributed to a change in surface properties of the ^{124}I conjugated ORMOSIL nanoparticles. In case of radiolabelled nanoparticles, the ^{124}I was conjugated on the outer surface of the nanoparticles via the surface NH_2 groups coupled to the Bolton hunter reagent. This might have resulted in the overall charge neutralization of the ORMOSIL nanoparticles and thus a different zeta potential value for the ^{124}I tagged ORMOSIL nanoparticles and thus different surface properties.

It is also worthwhile to note that the half life of the ^{124}I is sufficient to perform decay-corrected gamma counting till 2 weeks post injection. However, the ^{124}I was tagged on the surface of the nanoparticles via the amide bond, which is pretty much more susceptible to cleavage by the various enzymes (esterases/hydrolases) and thus more labile in *in vivo* conditions. Also as we have seen from the figure 2, the major accumulation of these ORMOSIL nanoparticles occur predominantly in liver, and it is well known that amides are hydrolyzed in the liver.[25] There are several other reports in the literature, which indicate the instability of the amide bonds in *in vivo* environment.[26-27] So the stability of the amide bond is the key concern for us to carry out the long term biodistribution studies with the ^{124}I tagged ORMOSIL nanoparticles. Once the bond will be cleaved it will be difficult to distinguish between the ^{124}I tagged to nanoparticles from free ^{124}I. On the other hand, in case of DY776 it is covalently conjugated inside the matrix of the ORMOSIL nanoparticles, which results in their reduced access to degrading enzymes and consequent higher physiological stability of these bonds. However, the rate of detachment of the linked probes may vary from species to species and also dependent on the surrounding environment. More rigorous analysis is required to further understand a precise mechanism involved in the detachment of these molecules from the nanoparticles.

As reported previously by several authors, the nanoparticle size, composition and surface characteristics determine their biodistribution profile and stability in the body.[28] It is well established that the particle size and surface composition plays a significant role in various physiological parameters such as hepatic filtration, tissue extravasation, tissue diffusion and kidney excretion.[3, 29-33] It has been shown that larger particles tend to accumulate more into the liver as compared to the smaller ones.[34] The enhanced uptake in the liver, spleen, and bone marrow is largely attributed to the macrophages residing in these tissues, which are responsible for capturing particulates and macromolecules circulating in the blood. When nanoparticles are systemically administered, a variety of serum proteins bind to their surface, which are recognized by the scavenger receptors on the macrophage cell surface and are removed from circulation.[35] The serum proteins binding to the nanoparticles are also termed “opsonins”, and the macrophages belong to the reticuloendothelial system (RES) or mononuclear phagocyte system (MPS) of the body.

The surface charge of the nanoparticles greatly affects the biodistribution of the nanoparticles. It is known that nanoparticles with neutral or zwitterionic behavior have a reduced plasma adsorption. Gbadamosi et al[36] successfully established a linear correlation between the surface charge of the nanoparticles and the extent of phagocytosis by the macrophage cells. The surface charge of the nanoparticles can be easily modulated using hydrophilic polymer poly(ethylene glycol) (PEG). It has been well established that PEG is a classical polymer with uncharged, hydrophilic and nonimmunogenic properties, which can be physically adsorbed or covalently attached to the surface of nanoparticles.[37] Furthermore, PEG has been shown to substantially reduce non-specific interactions with proteins through its hydrophilicity and steric repulsion effects, reducing opsonization.[38, 39] The chain length, shape and the density of PEG on the nanoparticle surface has been studied as the main parameters affecting nanoparticle's surface hydrophilicity and phagocytosis, and thus the biodistribution of the nanoparticles in the systemic circulation.

Figure 3 shows the data on the clearance of the DY776 conjugated ORMOSIL nanoparticles from a small batch of injected mice. The injected animals were imaged daily over a period 15 days. Free fluorophore DY776 was used as a control. It is quite evident from the figure 3 (upper panel) that animals injected with the nanoparticles initially showed a liver and spleen accumulation over a period of 24 hrs, whereas at 72 hrs post injection maximum fluorescence was acquired from the skin. Subsequent daily imaging with the same acquisition time revealed that fluorescence from the skin gradually kept on decreasing, beginning at 120 hrs post injection, reaching a minimum at 360 hrs post injection. In contrast, free DY776 injected under the same experimental conditions showed complete dominance of fluorescence from the skin as early as 24hrs post injection (figure 3, lower panels). The reason for the high affinity of free DY776 for skin is not known. Also, here the fluorescence from the skin kept on decreasing with time, and at 360 hrs post injection the fluorescence patterns for animals injected with both the free dye and the nanoconjugated dye appeared very similar. For a more quantitative estimation of fluorescence from the animals, three random time points (24hrs, 120hrs, and 360hrs post injection) were selected, where the mice were sacrificed and the fluorescence quantified from their harvested organs.

It is interesting to note that in the mice injected with the DY776 conjugated nanoparticles (figure 4a), the intensity of fluorescence (% of fluorescence of the injected dose) in the liver is reduced to almost post injection. Fluorescence was quantified as the percentage fluorescence intensity of the injected dose (from 75% at 24hrs to 37% at 120 hrs), whereas the intensity from the stomach increased several times (from 6% at 24hrs to 29% at 120hrs). This result indicates the excretion of the nanoparticles with the fecal matter via the hepatobiliary transport mechanism through the stomach. Previously, Renaud et al. reported that low-density lipoprotein-coated gold nanoparticles at 20nm diameter entered hepatocytes in the liver and were excreted through the fecal pathway.[40] Also, it is worthwhile to note that the intensity of fluorescence in the skin had also increased, which can be attributed to the release of the free fluorophore, indicating the degradation of the nanoparticles. The fluorescence intensity from the mice injected with free DY776 showed a typical accumulation pattern for small molecules. The maximum intensity after 24hrs post injection was observed from intestine (~47%), whereas the liver showed an intensity of 28%, followed by kidney (~15%), and skin (~9%). The fluorescence intensity after 360hrs in both the cases was maximum from the stomach and the intestine, which was ~3% (combined) in case of mice injected with the ORMOSIL nanoparticles and ~12% in control mice. Other organs like liver, spleen and skin accounts for ~1% (each) fluorescence intensity. This observation clearly suggests an initial uptake of the ORMOSIL nanoparticles by the RES system, followed by their gradual degradation and excretion via the hepatobiliary mechanism over a period of 15days.

Figure 5 shows the fluorescence images of the dissected mice injected with DY776, both free and conjugated with nanoparticles, recorded at 24, 120 and 360 hrs post-injection. It can be clearly visualized that fluorescence from the liver at 24hrs was maximum, which decreased after 120hrs and became negligible at 360hrs, whereas in the stomach it followed a reverse trend. These observations indicate excretion of the nanoparticles via the hepatobiliary transport mechanism.

In a similar study on the clearance of silica based nanoparticles from animals, Burns et al have shown that smaller sized nanoparticles (3-6 nm) can be effectively cleared out of the animal by renal excretion.[29] They have also seen the retention of the bigger sized (~30 nm) nanoparticles into the liver, which is quite similar to our biodistribution results. Since the particle size in our case is in the range of 20-25nm, glomerular filtration in kidney, which is primarily dependent on the size of the metabolites, is ineffective in their clearance. For larger metabolites, the preferred route of excretion is through the fecal matter, via the liver and the bile. Protein binding and phagocytosis by RES plays a critical role in removing the xenobiotic

metabolites from the plasma and delivering them to the liver, whereby they are degraded and excreted out as feces along with bile. The present observation of the fluorescence emission from the fecal matter suggests the degradation of the nanoparticles in the liver and spleen, which is similar to the studies done earlier using other nanoparticles.[40, 41]

For any of the existing clinically approved diagnostic formulations, the most favored route of excretion is still the renal route, as opposed to the hepatobiliary route. This is because the hepatobiliary excretion is a slow process, and long-term retention in the RES increases the likelihood of organ toxicity of the injected nanoparticles. Therefore, it is critical to ensure that the injected nanoparticles, prior to their fecal excretion, did not inflict any tissue/organ toxicity. For that, we have carried out histological analysis of the major organs (liver, spleen, kidney and lung) at 360 hrs post injection of the DY776 conjugated OMROSIL nanoparticles. Tissues were harvested and fixed in 10% neutral buffered formalin, processed routinely into paraffin, and 4μm sections were cut and stained with haematoxylin and eosin (H&E) and examined using light microscopy. As seen in Figure 6, no apparent tissue/cellular damages were observed in the mice injected with the DY776 conjugated nanoparticles, when compared to that obtained from mice injected with free DY776. Normal liver macrophages showed no evidence of cell injury. No pathological changes were observed in the spleen, kidney, liver, and lungs. Tissue sections were also studied for fluorescence; absence of any fluorescence from the tissues confirmed the clearance of the nanoparticles from these organs at 15 days post injection. Furthermore, mice injected with the ORMOSIL nanoparticles underwent physical and neurological evaluations for more than one month. No changes in eating, drinking, grooming, exploratory behavior, activity, physical features (e.g., weight and skin color), and neurological status were observed in these.

Conclusions

In summary, we report the synthesis of NIR fluorophore DY776 conjugated ORMOSIL nanoparticles by a simple normal micellar route, which can also be subsequently radiolabelled with Iodine-124. The biodistribution of the nanoparticles by NIR optical and radiolabelling studies suggests accumulation of the nanoparticles in the major RES organs in mice. The clearance studies of the injected nanoparticles have indicated that almost 100% of the nanoparticles were effectively cleared out of the animal via the hepatobiliary excretion, without any sign of organ toxicity. These studies provide preliminary answers to some of the key biological issues raised over the use and safety of the silica based nanoparticles for diagnostic and therapeutic applications. Overall, the results demonstrate the use of these NIR dye and Iodine-124 conjugated ORMOSIL nanoparticles as promising probes for safe *in vivo* bioimaging.

Experimental Section

Materials and Methods

ORMOSIL precursors vinyltriethoxysilane (VTES) and aminopropyltriethoxysilane (APTES), as well as the surfactant AOT were purchased from Sigma-Aldrich, and 2-[methoxy (polyethylenoxy)propyl]trimethoxy silane (PEG-silane) was procured form Gelest Inc. The NIR fluorophore DY776-*N*-succinimidyl ester (DY776-NHS) was obtained from Dyomics GmBH. The pancreatic cancer cell line Panc 1 was obtained from ATCC (Manassas, VA) and cultured according to vendor's instructions. Unless otherwise mentioned, all cell culture products and antibodies were obtained from Invitrogen.

Synthesis of DY776 conjugated ORMOSIL nanoparticles

Amino-terminated ORMOSIL nanoparticles with covalently incorporated NIR fluorophore, DY776, were synthesized in the non-polar core of an oil-in-water microemulsion, as per our earlier report but with a slight modification.[15] Briefly, 0.2 g of surfactant AOT and 300 μl of n-butanol and 100 μl of DMSO were dissolved in 10ml HPLC grade water by magnetic stirring. To this microemulsion system, 100 μl of 1mg/ml of DY776-silane precursor (DY776 NHS ester, conjugated to aminopropyltriethoxy silane; scheme 1a) in DMSO was added and stirred, followed by an addition of 100 μl of neat VTES. The reaction mixture was stirred for another hour and polymerization reaction was started by the addition of 10 μl of amino-propyltriethoxysilane. For incorporation of the PEG molecules on the surface of the nanoparticles, 10 μl of PEG silane was added after 30min of stirring. The final reaction mixture was allowed to stir overnight. The mixture was then dialyzed against distilled water for 48h at room temperature, using a cellulose membrane with a cut-off size of 12-14 kD. Following dialysis, the nanoparticles were sterile filtered and stored at 4 °C for future use.

^{124}I radiolabelling of ORMOSIL nanoparticles

The radiolabeling protocol is an adaptation of the well known Bolton-Hunter method, whereby the free amino groups on the nanoparticle surface will form a covalent linkage with the N-hydroxysuccinimide (NHS) ester group linked with ^{124}I (^{124}I-NHS).[42] For the synthesis of ^{124}I-NHS, ^{124}I was distilled and dried in a small reaction vial (0.3 ml, Wheaton, USA). A solution of NaI carrier (5 μl, 89.2 μM), HCl (14 μl, 100 mM), and sodium phosphate buffer (10 μl, 250 mM, pH 7.4) was added to ^{124}I (14 μl, 370 MBq). The reaction was allowed to incubate at room temperature for 10 minutes. SHPP (*N*-Succinimidyl-3-[4-hydroxyphenyl] propionate in 1,4-dioxane, 2 μl, 3.8 mM) and Chloramine-T (10 μl, 22 mM), dissolved in sodium phosphate buffer (250 mM, pH 7.4), were added with mixing and the reaction was terminated immediately (~15 seconds) with a sodium phosphate buffered solution (250 mM, pH 7.4) of $Na_2S_2O_5$ (10 μl, 63 mM). The reaction product was extracted with benzene/dimethylfluoride (100 μl, 40:1 v/v), dried with 30 mg Na_2SO_4, and transferred into another reaction vessel (scheme 2).

For conjugation with the nanoparticles, the solvent was evaporated with a stream of nitrogen and 2ml of amino-terminated ORMOSIL nanoparticle dispersion was added. The solution was left for stirring overnight at room temperature. The final dispersion of radiolabelled ORMOSIL nanoparticles was purified from any non-reacted ^{124}I-NHS by dialysis using a cellulose membrane with a cut-off size of 12-14 kD for 24h at room temperature.

Animal model

Animal experiments were conducted in agreement with all relevant guidelines and regulations set by the University at Buffalo, and with approved institutional protocols by the American Association of Laboratory Animal Care. Six-to-seven week old female athymic nude mice (Hsd:Athymic Nude-*Foxn1*^{nu}) were procured from Harlan Sprague Dawley Inc., and were housed in a group of five in standard cages with free access to food and water and a 12 hrs light/dark cycle. All animals acclimated to the animal facility for at least 48 hrs before experimentation. All possible parameters that may cause social stress, like group size, type (treated and non treated) etc., among the experimental animals were carefully monitored and avoided. Animals were observed daily for any behavioral abnormalities and weighed weekly.

ORMOSIL nanoparticles biodistribution and clearance studies

For biodistribution and clearance studies, isotonic dispersion (5% glucose) of the above-synthesized ORMOSIL nanoparticles (non-radiolabelled) were injected intravenously in nude mice (n=3) at a concentration of 2.0 mg/kg body weight. For the control group (n=3) of mice,

DY776-NHS ester was injected i.v. after matching their absorbance with that of DY776 conjugated with ORMOSIL nanoparticles. Also, 100 μl of sterile PBS was injected i.v. into a negative control mice group. The mice were imaged every 24 hrs till 15 days, using the Maestro GNIR FLEX fluorescence imaging system (CRi) (for details, see Supporting information). The NIR fluorophore DY776 was excited using a "NIR" excitation filter (CRi), transmitting light from the source (Xe lamp) in the range of 710-760nm. An NIR emission filter (800 LP) in front of the imaging CCD camera was used to cut off the excitation light. The images were acquired with the same acquisition time of 623ms for all the experimental animals. A quantitative estimation of the fluorescence intensity was done using the Maestro software. For probing any potential *in vivo* toxicity of the injected nanoparticles, the mice were anesthetized and sacrificed at different intervals, and major organs such as liver, spleen, kidney, lungs, heart and skin were dissected out for further histological analysis.

For biodistribution studies using the ^{124}I labeled and dye-doped ORMOSIL nanoparticles, 200 μCi of radiolabeled nanoparticles were injected intravenously through tail vein in mice (n=3). MicroPET imaging was carried out with a microPET camera, Focus 120® (Siemens Concorde Microsystems, previously CTI Concorde Microsystems). Before scanning, the mice were anesthetized with O_2/isoflurane (1%-3% isoflurane). The mouse was imaged in the prone position in the gantry of the microPET scanner and was scanned for 30 minutes. The emission scan window was set between 350 – 750 keV and the analysis of the acquired data and image reconstruction was done with 2D filtered back projection, using the software microPET manager 2.2.4.0. The mice was imaged and sacrificed at 10min and 24h post injection. Organs of interest (tumor, heart, liver, spleen, lungs, muscle, gut, kidney, blood and stomach) were immediately dissected out and weighed for quantitative estimation of gamma counts from the ^{124}I conjugated to ORMOSIL nanoparticles using a gamma scintillator. Radioactivity obtained from different organs was calculated as the percentage of the injected dose per gram of the tissue (%ID/g).

Histological Analysis

For histochemical studies, the major organs such as liver, spleen, kidney, heart, lung, and skin were harvested, and fixed in 10% neutral buffered formalin. Following that, they were embedded in paraffin, and approximately 4um thick sections were cut and stained with hematoxylin and eosin (H&E). The histological sections were observed under an optical microscope with different combinations of magnification and objective lens. Micrographs of the sections were recorded for comparison.

Supplementary Material

Refer to Web version on PubMed Central for supplementary material.

Acknowledgments

This study was supported by NIH Grants CA119397 and CA104492 and the John R. Oishei Foundation. We thank Dr. Weiwei Zhao for kind help in histological studies.

References

1. Kobyashi H, Brechbiel M. Nano-Sized Mri Contrast Agents With Dendrimer Cores. Adv Drug Delivery Rev 2005;57:2271–2286.
2. Prasad, PN. Introduction To Biophotonics. Wiley-Interscience; New York: 2004.
3. Choi HS, Liu W, Misra P, Tanaka E, Zimmer JP, Ipe BI, Bawendi MG, Frangioni JV. Renal Clearance Of Quantum Dots. Nat Biotechnol 2007;25:1165–1170. [PubMed: 17891134]

4. Sevick-Muraca E, Houston J, Gurfinkel M. Fluorescence-enhanced, Near Infrared Diagnostic Imaging With Contrast Agent. Curr Opin Chem Biol 2002;6:642–650. [PubMed: 12413549]
5. Frangioni JV. *In Vivo* Near-Infrared Fluorescence Imaging. Curr Opin Chem Biol 2003;7:626–634. [PubMed: 14580568]
6. Wagner V, Dullaart A, Bock AK, Zweck A. The Emerging Nanomedicine Landscape. Nat Biotechnol 2006;24:1211–1217. [PubMed: 17033654]
7. Kim S, Lim YT, Soltesz EG, De Grand AM, Lee J, Nakayama A, Parker JA, Mihaljevic T, Laurence RG, Dor DM, Cohn LH, Bawendi MG, Frangioni JV. Near-Infrared Fluorescent Type Ii Quantum Dots For Sentinel Lymph Node Mapping. Nat Biotechnol 2004;22:93–97. [PubMed: 14661026]
8. Nyk M, Kumar R, Ohulchanskyy TY, Bergey EJ, Prasad PN. High Contrast *In Vitro* and *In Vivo* Photoluminescence Bioimaging Using Near Infrared to Near Infrared Up-Conversion in Tm^{3+} and Yb^{3+} Doped Fluoride Nanophosphors. Nano Lett 2008;8:3834–3838. [PubMed: 18928324]
9. Deissler V, Ruger R, Frank W, Fahr A, Kaiser WA, Hilger I. Fluorescent Liposomes As Contrast Agents For *In Vivo* Optical Imaging Of Edemas In Mice. Small 2008;4:1240–1246. [PubMed: 18666163]
10. Ghoroghchian PP, Frail PR, Susumu K, Blessington D, Brannan AK, Bates FS, Chance B, Hammer DA, Therien MJ. NIR-Emissive Polymersomes: Self-assembled Soft Matter For *In Vivo* Optical Imaging. Proc Natl Acad Sci USA 2005;102:2922–2927. [PubMed: 15708979]
11. Altinoglu EI, Russin TJ, Kaiser JM, Barth BM, Eklund PC, Kester M, Adair JH. Near-Infrared Emitting Fluorophore-Doped Calcium Phosphate Nanoparticles for *In Vivo* Imaging of Human Breast Cancer. ACS Nano 2008;2:2075–2084. [PubMed: 19206454]
12. Josephson L, Kircher MF, Mahmood U, Tang Y, Weissleder R. Near-infrared Fluorescent Nanoparticles As Combines Mr/Optical Imaginprobes. Bioconjugate Chem 2002;13:554–560.
13. Park JH, von Maltzahn G, Ruoslahti E, Bhatia SN, Sailor M. Micellar Hybrid Nanoparticles for Simultaneous Magnetofluorescent Imaging and Drug Delivery. J Angew Chem Int Ed 2008;47:7284–7288.
14. Kumar R, Ohulchanskyy TY, Roy I, Gupta SK, Borek C, Thompson ME, Prasad PN. Near-Infrared Phosphorescent Polymeric Nanomicelles: Efficient Optical Probes for Tumor Imaging and Detection. ACS Appl Mater Interfaces 2009;1:1474–1481.
15. Kumar R, Roy I, Ohulchanskyy TY, Goswami LN, Bonoiu AC, Bergey EJ, Tramposch M, Maitra A, Prasad PN. Covalently Dye-linked, Surface-controlled, and Bioconjugated Organically Modified Silica Nanoparticles As Targeted Probes For Optical Imaging. ACS Nano 2008;2:449–456. [PubMed: 19206569]
16. Selvan ST, Tan TT, Ying JY. Robust, Non-Cytotoxic, Silica-Coated CdSe Quantum Dots with Efficient Photoluminescence. Adv Mat 2005;17:1620–1625.
17. Ow H, Larson DR, Srivastava M, Baird BA, Webb WW, Wiesner U. Bright and Stable Core-Shell Fluorescent Silica Nanoparticles. Nano Lett 2005;5:113–117. [PubMed: 15792423]
18. Zhao X, Hilliard LR, Menchery SJ, Wang Y, Bagwe RP, Jin S, Tan W. A Rapid Bioassay for Single Bacterial Cell Quantitation Using Bioconjugated Nanoparticles Proc. Natl Acad Sci USA 2004;101:15027–15032.
19. Santra S, Liesenfeld B, Dutta D, Chatel D, Batich CD, Tan W, Moudgil BM, Mericle RA. Folate Conjugated Fluorescent Silica Nanoparticles for Labeling Neoplastic Cells. J Nanosci Nanotechnol 2005;5:899–904. [PubMed: 16060150]
20. Law WC, Yong KT, Roy I, Xu ZX, Ding H, Bergey EJ, Zeng H, Prasad PN. Optically And Magnetically Doped Organically Modified Silica Nanoparticles As Efficient Magnetically Guided Biomarkers for Two-photon Imaging Of Live Cancer Cells. J Phys Chem C 2008;112:7972–7977.
21. Bharali DJ, Klejbor I, Stachowiak EK, Dutta P, Roy I, Kaur N, Bergey EJ, Prasad PN, Stachowiak MK. Organically Modified Silica Nanoparticles: A Nonviral Vector for *In Vivo* Gene Delivery And Expression in the Brain. Proc Natl Acad Sci U S A 2005;102:11539–11544. [PubMed: 16051701]
22. Roy I, Ohulchanskyy TY, Pudavar HE, Bergey EJ, Oseroff AR, Morgan J, Dougherty TJ, Prasad PN. Ceramic-Based Nanoparticles Entrapping Water-Insoluble Photosensitizing Anticancer Drugs: A Novel Drug-Carrier System for Photodynamic Therapy. J Am Chem Soc 2003;125:7860–7865. [PubMed: 12823004]

23. Weissleder R. A Clearer Vision for *In Vivo* Imaging. Nat Biotechnol 2001;19:316–317. [PubMed: 11283581]
24. Chan WCW, Maxwell DJ, Gao X, Bailey RE, Han M, Nie S. Luminescent Quantum Dots For Multiplexed Biological Detection And Imaging. Curr Opin Biotechnol 2002;13(1):40–46. [PubMed: 11849956]
25. Greenwald RB, Zhao H, Peng P, Longley CB, Dai QH, Xia J, Martinez A. An Unexpected Amide Bond Cleavage: Poly (ethylene glycol) transport Forms of Vanomycin. Eur J Med Chem 2005;40:798–804. [PubMed: 16122582]
26. Koeplinger KA, Zhao Z, Peterson T, Leone JW, Schwende FS, Heinrikson RL, Tomasselli AG. Activated Sulfonamides are Cleaved by Glutathione-s-Transferases. Drug Metab Dispos 1999;27:986–991. [PubMed: 10460796]
27. Weber, WW.; Levy, GN.; Hein, DW. Acetylation, in Conjugation Reactions in Drug Metabolism: An Integrated Approach. Mulder, GJ., editor. Taylor and Francis; New York: 1990. p. 178-180.
28. Alexis F, Pridgen E, Molnar LK, Farokhzad OC. Factors Affecting the Clearance and Biodistribution of Polymeric Nanoparticles. Mol Pharm 2008;5:505–515. [PubMed: 18672949]
29. Burns AA, Vider J, Ow H, Herz E, Penate-Medina O, Baumgart M, Larson SM, Wiesner U, Bradbury M. Fluorescent Silica Nanoparticles With Efficient Urinary Excretion For Nanomedicine. Nano Lett 2009;9:442–444. [PubMed: 19099455]
30. Fischer HC, Liu L, Pang KS, Chan WCW. Pharmacokinetics of Nanoscale Quantum Dots: *In Vivo* Distribution, Sequestration, and Clearance in the Rat. Adv Funct Mater 2006;16:1299–1305.
31. Schipper ML, Ratchford NN, Davis CR, Kam NW, Chu P, Liu Z, Sun X, Dai H, Gambhir SS. A Pilot Toxicology Study of Single-walled Carbon Nanotubes in a Small Sample of Mice. Nat Nanotech 2008;3:216–221.
32. Yong KT, Roy I, Ding H, Bergey EJ, Prasad PN. Biocompatible Near-Infrared Quantum Dots as Ultrasensitive Probes for Long-Term. In Vivo Imaging Applications Small 2008;5:1997–2004.
33. Jain TK, Reddy MK, Morales MA, Leslie-Pelecky DS, Labhasetwar V. Biodistribution, Clearance, And Biocompatibility Of Iron Oxide Magnetic Nanoparticles In Rats. Mol Pharm 2008;5:316–327. [PubMed: 18217714]
34. Nagayama S, Ogawara K, Fukuoka Y, Higaki K, Kimura T. Time-Dependent Changes In Opsonin Amount Associated On Nanoparticles Alter Their Hepatic Uptake Characteristics. Int J Pharm 2007;342:215–221. [PubMed: 17566676]
35. Opanasopit P, Nishikawa M, Hashida M. Factors Affecting Drug and Gene Delivery: Effects of Interaction with Blood Components. Crit Rev Ther Drug Carrier Syst 2002;19:191–233. [PubMed: 12627613]
36. Gbadamosi JK, Hunter AC, Moghimi SM. PEGylation of Microspheres Generates A Heterogeneous Population Of Particles With Differential Surface Characteristics And Biological Performance. FEBS Lett 2002;532:338–344. [PubMed: 12482589]
37. Mosqueira VCF, Legrand P, Gulik P, Bourdon O, Gref R, Labarre D, Barratt G. Relationship Between Complement Activation, Cellular Uptake And Surface Physicochemical Aspects Of Novel Peg-Modified Nanocapsules. Biomaterials 2001;22:2967–2979. [PubMed: 11575471]
38. Bazile D, Prudhomme C, Bassoullet MT, Marlard M, Spenlehauer G, Veillard M. Stealth Me.PEG-PLA Nanoparticles Avoid Uptake By The Mononuclear Phagocytes System. J Pharm Sci 1995;84:493–498. [PubMed: 7629743]
39. Li Y, Pei X, Zhang Z, Gu Z, Zhou W, Yuan J, Zhou J, Zh, Gao X. PEGylated PLGA Nanoparticles As Protein Carriers: Synthesis, Preparation And Biodistribution In Rats. J Controlled Release 2001;71:203–211.
40. Renaud G, Hamilton RL, Havel RJ. Hepatic Metabolism Of Colloidal Gold-Low-Density Lipoprotein Complexes In The Rat: Evidence For Bulk Excretion Of Lysosomal Contents Into Bile. Hepatology 1989;9:380–392. [PubMed: 2920994]
41. Choi J, Burns A, Williams R, Zhou Z, Flesken-Nikitin A, Zipfel W, Wiesner U, Nikitin A. Core-Shell Silica Nanoparticles As Fluorescent Labels For Nanomedicine. J Biomed Opt 2007;12:064007. [PubMed: 18163823]
42. Collingridge DR, Carroll VA, Glaser M, Aboagye EO, Osman S, Hutchinson OC, Barthel H, Luthra SK, Brady F, Bicknell R, Price P, Harris AL. The Development Of [(124)I]Iodinated-Vg76e: A Novel

Tracer For Imaging Vascular Endothelial Growth Factor *In Vivo* Using Positron Emission Tomography. Cancer Res 2002;62:5912–5919. [PubMed: 12384557]

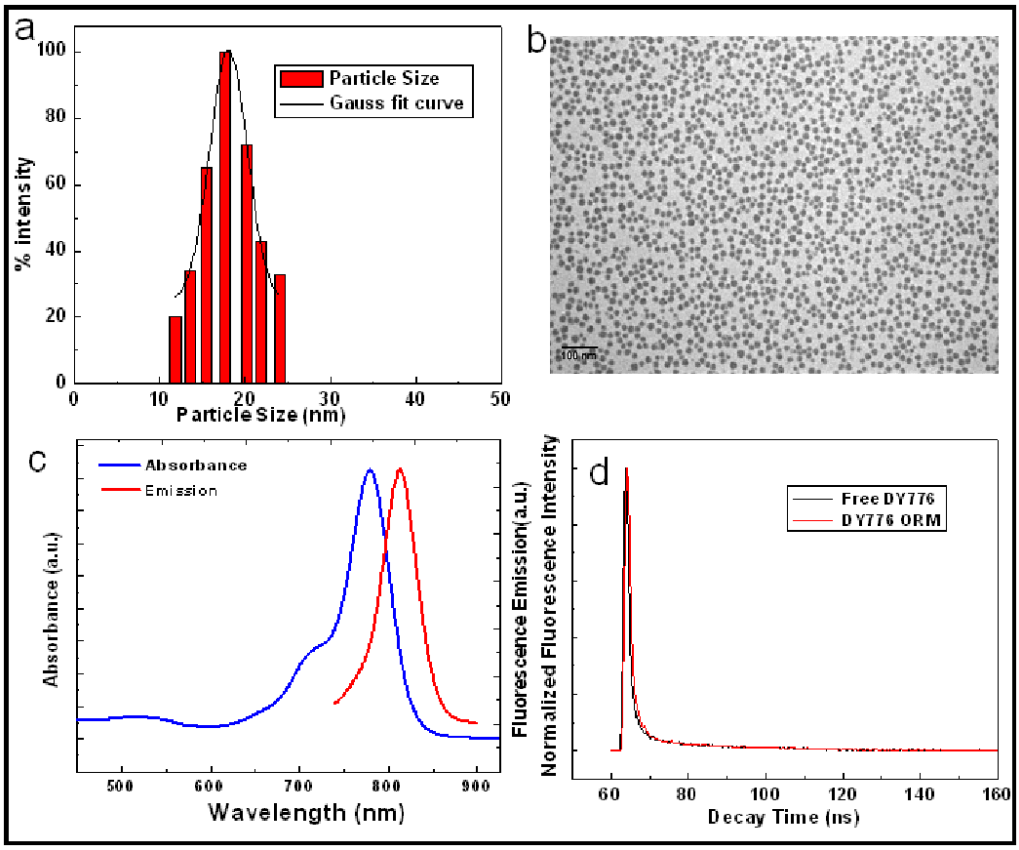

Figure 1.

Showing the basic characterization of the DY776 conjugated ORMOSIL nanoparticles: (1a) Nanoparticles size distribution profile as measured by DLS, (1b) representative TEM image, (1c) Absorption and emission spectra, (1d) fluorescence life time decay curves of the DY776, either free or conjugated with ORMOSIL nanoparticles.

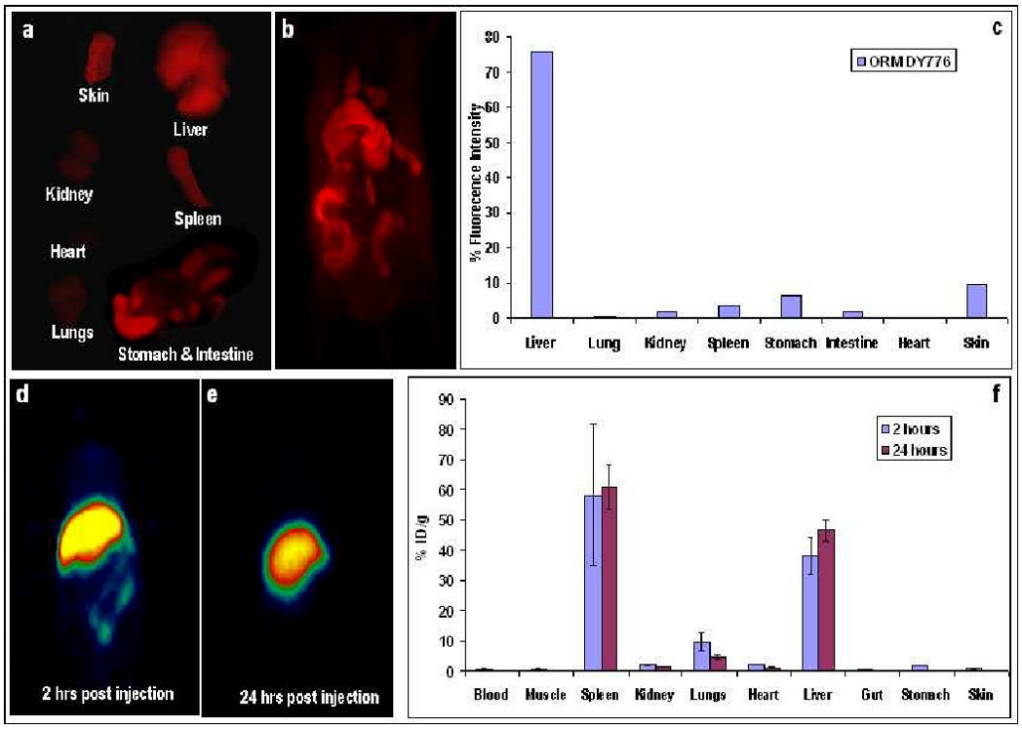

Figure 2.

Biodistribution of OMROSIL nanoparticles by the measurement of the fluorescence (a, b, c) and radioactivity (d, e, f) from different organs of the mice injected with DY776 conjugated and ^{124}I labeled ORMOSIL nanoparticles respectively. (a) fluorescence acquired from the individual organs, (b) whole body fluorescence imaging of the mice 24hrs post injection, (c) quantitative estimation of fluorescence acquired from different organs of the mice, (d & e) PET images of the mice injected with ^{124}I-ORMOSIL nanoparticles 2 and 24hrs post injection, respectively, and (f) quantitative radioactivity measurements from the individual organs of the mice.

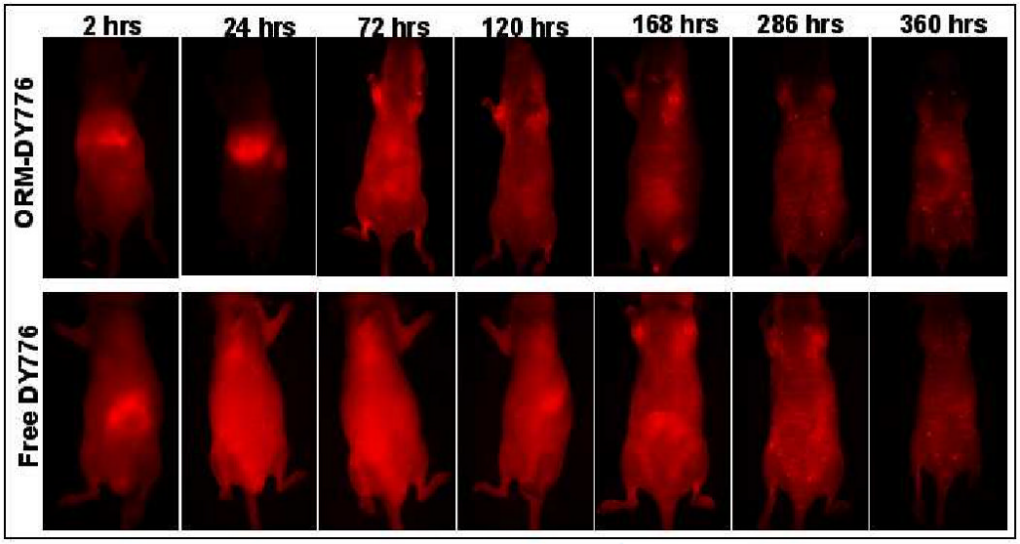

Figure 3.
Clearance of the DY776 conjugated ORMOSIL nanoparticles injected intravenously into the mice (upper panel) and a comparison with the free DY776 injected mice as control (lower panel). Same acquisition time was maintained for all the time points of imaging.

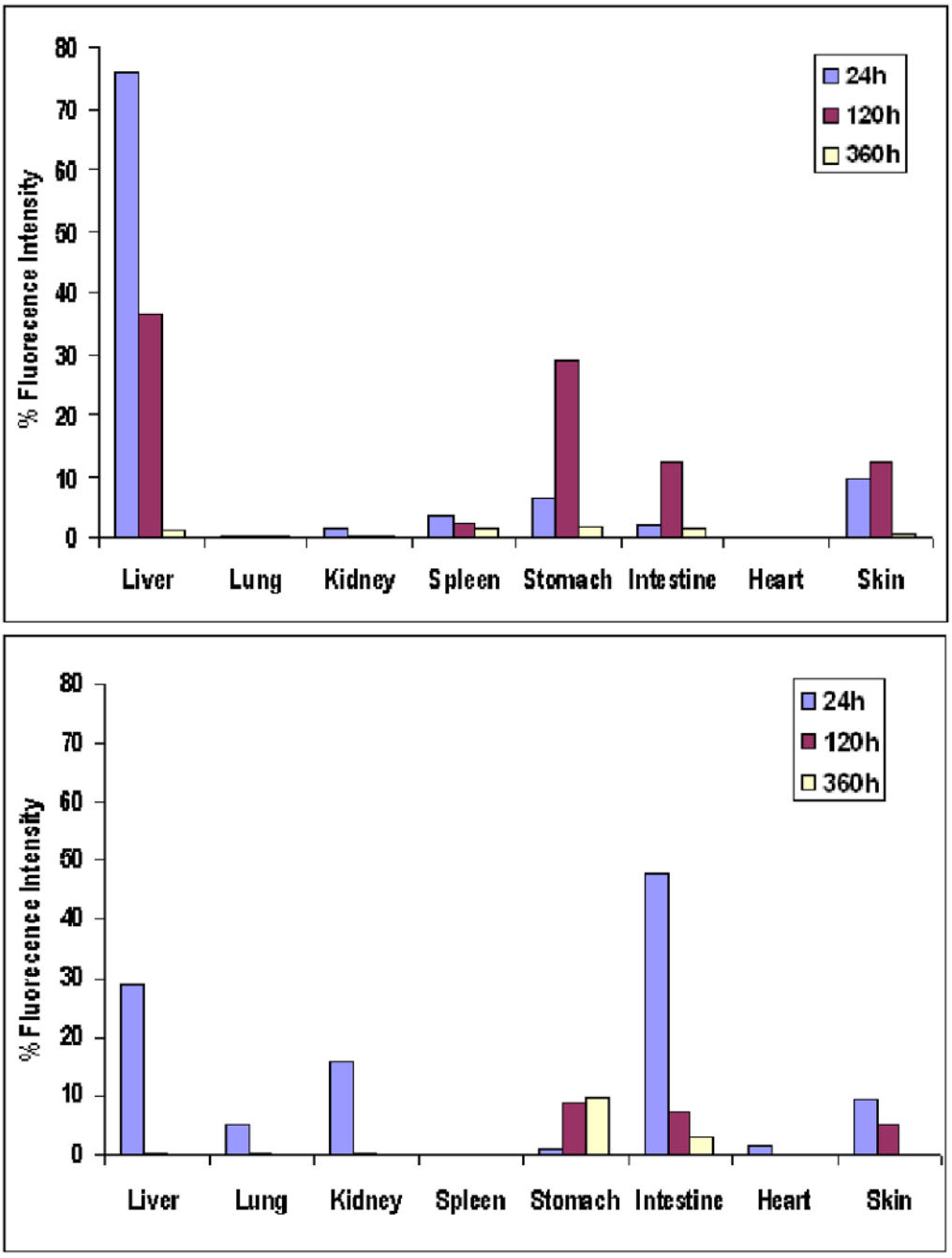

Figure 4.
Quantitative estimation of fluorescence acquired from various organs of the mice injected with (a) the DY776 conjugated ORMOSIL nanoparticles and (b) free DY776, at 24, 120 and 360 hrs.

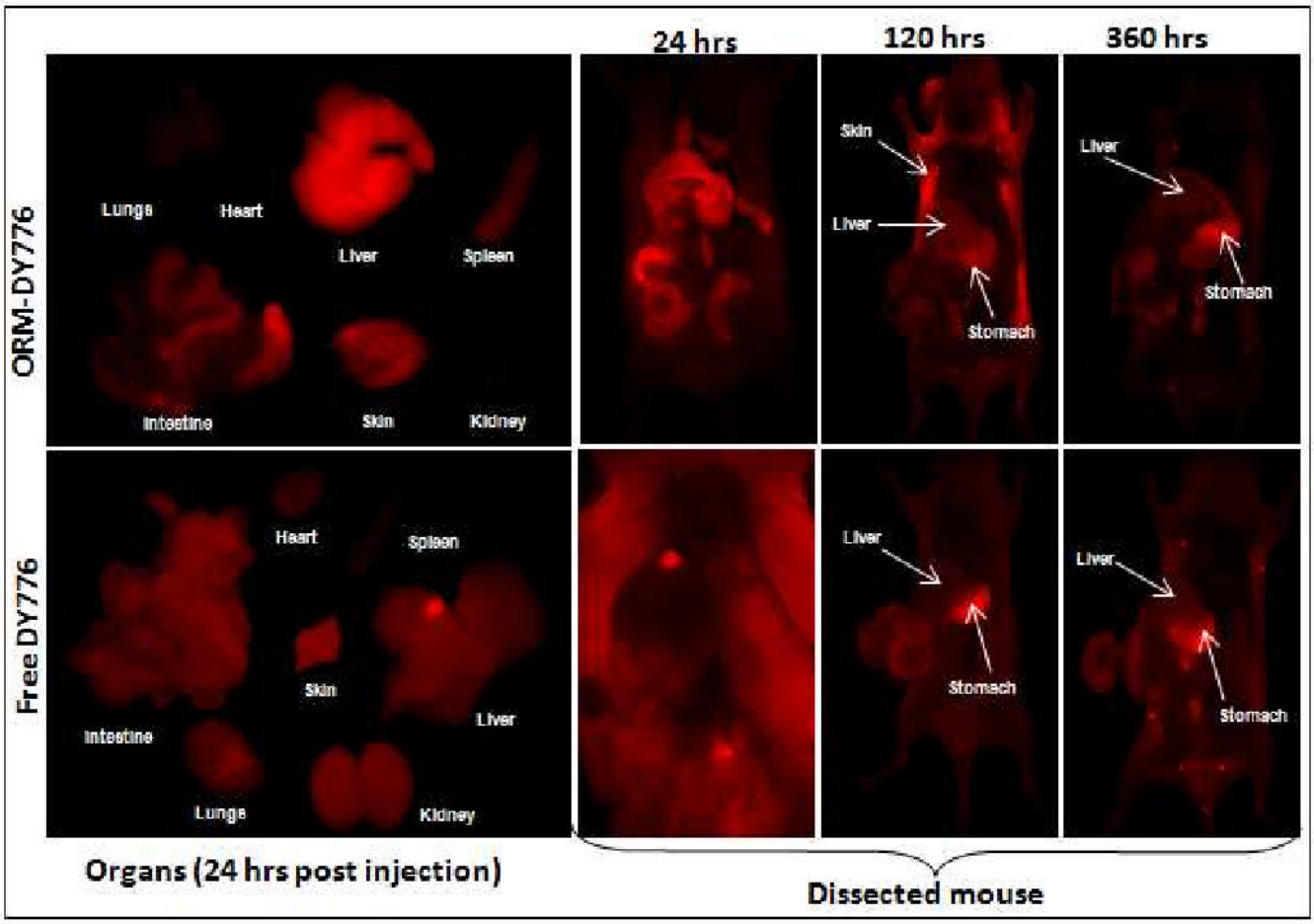

Figure 5.

Fluorescence images of the organs as well as dissected mice injected with the DY776 conjugated ORMOSIL nanoparticles (upper panel) and free DY776 (lower panel) at 24, 120 and 360 hrs post-injection. A gradual reduction in the fluorescence intensity indicates excretion of the nanoparticles by the hepatobiliary route.

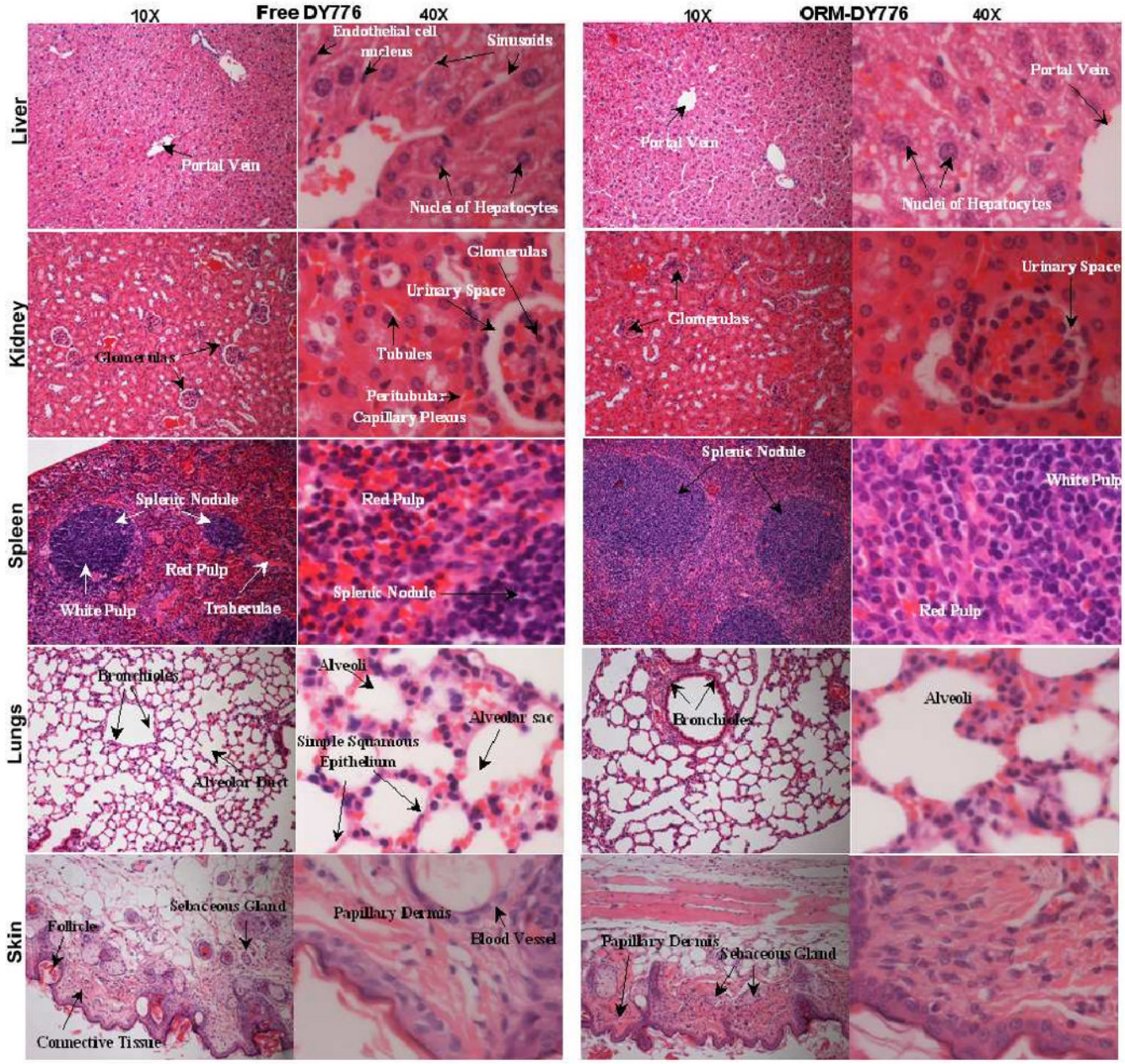

Figure 6.

Histological sections of liver, kidney, spleen, lungs and skin samples, collected after 15 days post injections of the free DY776 (left) and DY776 conjugated ORMOSIL nanoparticles (right). Sections were stained with H&E and observed under a light microscope at 10× and 40× magnification.

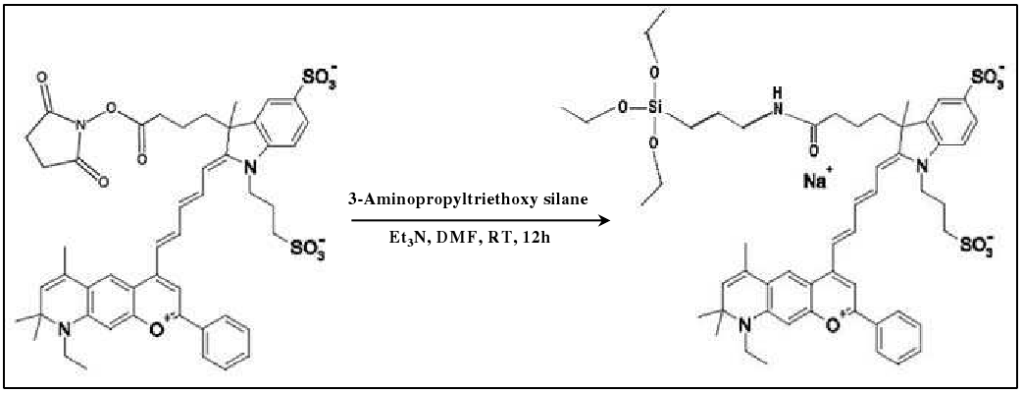

Scheme 1.
Coupling of silane precursor, 3-aminopropyltriethoxy silane, to DY776 NHS ester to form DY776 silane precursor.

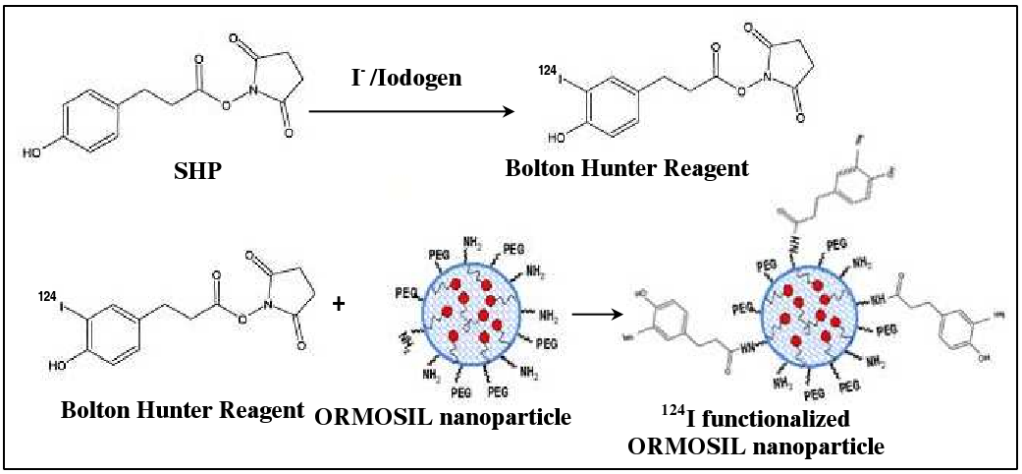

Scheme 2.
Synthesis of ^{124}I labeled DY776-conjugated ORMOSIL nanoparticles via the Bolton Hunter method.